

Geophysical Research Letters

RESEARCH LETTER

10.1029/2019GL085891

Key Points:

- The interannual (2- to 7-year band) precipitation in Southern California is closely related to ENSO variance originating from the tropical Pacific
- Extratropical pressure systems modulate the interannual precipitation changes in Southern California by influencing the ENSO teleconnection
- The magnitude and frequency of interannual precipitation variance in Southern California changes throughout the past 2,000 years

Correspondence to:

X. Du,
xjdu@umich.edu

Citation:

Du, X., Hendy, I., Hinnov, L., Brown, E., Schimmelmann, A., & Pak, D. (2020). Interannual Southern California precipitation variability during the Common Era and the ENSO teleconnection. *Geophysical Research Letters*, 47, e2019GL085891. <https://doi.org/10.1029/2019GL085891>

Received 23 OCT 2019

Accepted 20 DEC 2019

Accepted article online 17 DEC 2019

Interannual Southern California Precipitation Variability During the Common Era and the ENSO Teleconnection

Xiaojing Du¹, Ingrid Hendy¹, Linda Hinnov², Erik Brown³, Arndt Schimmelmann⁴, and Dorothy Pak⁵

¹Department of Earth and Environmental Sciences, University of Michigan, Ann Arbor, MI, USA, ²Department of Atmospheric, Oceanic, and Earth Sciences, George Mason University, Fairfax, VA, USA, ³Large Lakes Observatory and Department of Earth and Environmental Sciences, University of Minnesota, Duluth, Duluth, MN, USA, ⁴Department of Earth and Atmospheric Sciences, Indiana University, Bloomington, IN, USA, ⁵Marine Science Institute, University of California, Santa Barbara, CA, USA

Abstract Southern California's Mediterranean-type hydroclimate is highly variable on interannual time scales due to teleconnected climate forcings such as the El Niño–Southern Oscillation (ENSO). Here we present subannually resolved scanning X-ray fluorescence Ti counts from deep-sea cores in Santa Barbara Basin, California, recording 2,000 years of hydroclimate variability. The reconstructed Southern California precipitation record contains interannual variability in the 2- to 7-year band that could be driven by changes in tropical Pacific ENSO variability and/or the strength of the ENSO teleconnection modulated by extratropical pressure systems. Observed interannual precipitation variance increased and was associated with longer periodicities (5–7 years) when the Intertropical Convergence Zone migrated southward (1370–1540 CE) and the Aleutian Low strengthened creating a robust ENSO teleconnection. Weak interannual precipitation variance with shorter periodicity (2–3 years) was observed when the Intertropical Convergence Zone shifted northward (700–900 CE) and/or the Aleutian Low was weak (1540–1680 CE).

Plain Language Summary El Niños occur when the rising branch of atmospheric circulation in the tropical Pacific shifts eastward, driving changes in air temperature and rainfall around the globe. Rainfall in Southern California often increases during El Niño events causing rivers to carry extra sediment to the ocean. We reconstructed Southern California rainfall for every year of the last 2,000 years using the elemental signature of river sediment deposited in Santa Barbara Basin. We found that after ~1350 CE, when the Aleutian Low was strong, interannual rainfall in Southern California varied more and with longer cycles (5 to 7 years). During this time, the region of rising air at the equator was further south and storms over the North Pacific Ocean were stronger and occurred further east. Both of these changes in atmospheric circulation increased the Southern California rainfall response to El Niño events in the tropical Pacific Ocean.

1. Introduction

The El Niño–Southern Oscillation (ENSO) drives a significant portion of interannual temperature and precipitation variability around the globe through “teleconnections.” The origin of El Niño and its opposite phase—La Niña—is attributed to internal atmosphere-ocean interactions (Cane & Zebiak, 1985); however, short-term radiative forcing from volcanic and solar variability has also been implicated (Emile-Geay et al., 2008; Mann et al., 2005). An ENSO teleconnection is a statistically significant climate response in a region distal to the ENSO forcing region in the equatorial Pacific. Understanding both ENSO variability and its global teleconnections requires long-duration high-resolution reconstructions during different background climates. Yet continuous multimillennial sediment records often lack the annual resolution required for resolving ENSO frequencies (Conroy et al., 2008) and/or suffer from poor age control (Moy et al., 2002). Fossil coral sequences provide well-dated high temporal-resolution (monthly to seasonal) records (Cobb et al., 2003) but lack the duration to reconstruct continuous multi-centennial to millennial-scale records. In spite of these spatial and temporal limitations, paleoclimate

reconstructions indicate considerable natural ENSO variability during the last millennium (Cobb et al., 2003; Emile-Geay et al., 2013; Rustic et al., 2015).

The Mediterranean-type hydroclimate of Southern California results in limited water resources. Precipitation in southern California is highly variable, increasing the difficulty of managing the region's limited water resources. The tropics impact Southern California precipitation through an ENSO teleconnection; increased tropical mean zonal sea surface temperatures (SSTs) enhance tropical convection during El Niño events, producing stronger upper tropospheric tropical divergence and subtropical convergence that shifts the midlatitude jet southward to bring more moisture to Southern California (Seager et al., 2010; Trenberth et al., 1998). Simultaneously, an eastward shift of a deepened Aleutian Low (AL) advects warm, moist air onto North America, enhancing precipitation events in Southern California (Trenberth et al., 1998).

Here we present a subannually resolved precipitation record from Southern California for the last 2,000 years and explore tropical and extratropical forcing of the interannual variability in the record. The precipitation reconstruction is generated by ITRAX scanning X-ray fluorescence (XRF) Ti counts at 0.2-mm sampling intervals or 4–7 data points per year from box core SPR0901-04BC (588-m water depth; 34°16.895'N, 120°02.489'W) and kasten core SPR0901-03KC (591-m water depth; 34°16.914'N, 120°02.419'W) collected in Santa Barbara Basin (SBB), CA. Titanium is relatively immobile during chemical weathering, making the element an indicator of terrigenous detrital input to sediments (Haug et al., 2001). Annual precipitation variability is captured when terrestrial siliciclastic sediment is transported into SBB by river runoff, which only occurs when precipitation events exceed 0.25 cm (Nezlin et al., 2005). Thus, Ti in SBB sediments is significantly correlated with regional observed precipitation, including events associated with 20th-century El Niño, and can be used to reconstruct Southern California hydroclimate (Hendy et al., 2015; Napier & Hendy, 2016). ^{14}C -based chronology was generated employing Bacon 2.2 (Blaauw & Christen, 2011) with a variable reservoir ages and the Marine13 calibration curve (Du et al., 2018; Hendy et al., 2013) (Figure S1 and Table S1). Ti peaks associated with winter siliciclastic laminae deposits were counted to produce an annually tuned chronology that is used to identify ENSO band periodicity. During droughts, winter siliciclastic laminae are not deposited in SBB, resulting in missing years in this annual tuned chronology. For this reason, the ^{14}C chronology is employed to determine absolute ages with annual tuning providing dating error estimates of <30 years.

2. Correlation Between Southern Californian Interannual Precipitation and ENSO Variability

Historical observations and models have related interannual winter precipitation variability in Southern California to ENSO (Jong et al., 2016; Seager et al., 2010; Trenberth et al., 1998). A field correlation between extended winter (November–April) Pacific SST from 100°E to 100°W and 26°S to 66°N, and instrumental precipitation in Southern California (122°–114°W, 32°–36°N) from 1900 to 2013 further supports this relationship (Figure 1; SST data are from National Oceanic and Atmospheric Administration Extended Reconstructed Sea Surface Temperature dataset version 4 (Huang et al., 2015); precipitation data are from Global Precipitation Climatology Centre Full Data Reanalysis version 6 (Schneider et al., 2014)). Winter precipitation in Southern California is positively correlated ($p < 0.013$; region encompassed by the dashed line in Figure 1a) to SSTs in both the central and eastern tropical Pacific, and the eastern North Pacific, and negatively correlated with SSTs in the central North Pacific Ocean. When a 2- to 7-year bandpass filter was applied to examine the correlation coefficient on an interannual scale, the significantly correlated ($p < 0.013$) regions in the North Pacific shrink (Figure 1b). Consequently, the central and eastern tropical Pacific (the core region of the ENSO SST anomalies and ENSO index regions including Niño 3.4, 3, and 4) dominate the correlation between SSTs and precipitation on interannual time scales. Thus, Southern California winter precipitation increases when the central and eastern tropical Pacific Ocean warms, and the western tropical Pacific cools, similar to the El Niño SST pattern (Figure 1b).

We further explored whether the relationship with Southern California precipitation and ENSO persisted in the sedimentary archive of river runoff by comparing 20th-century Ti counts from SBB sediments (SPR0901-04BC) with the Niño 3.4 SST anomalies (Figures 1c, 1d, and S2). A statistically significant

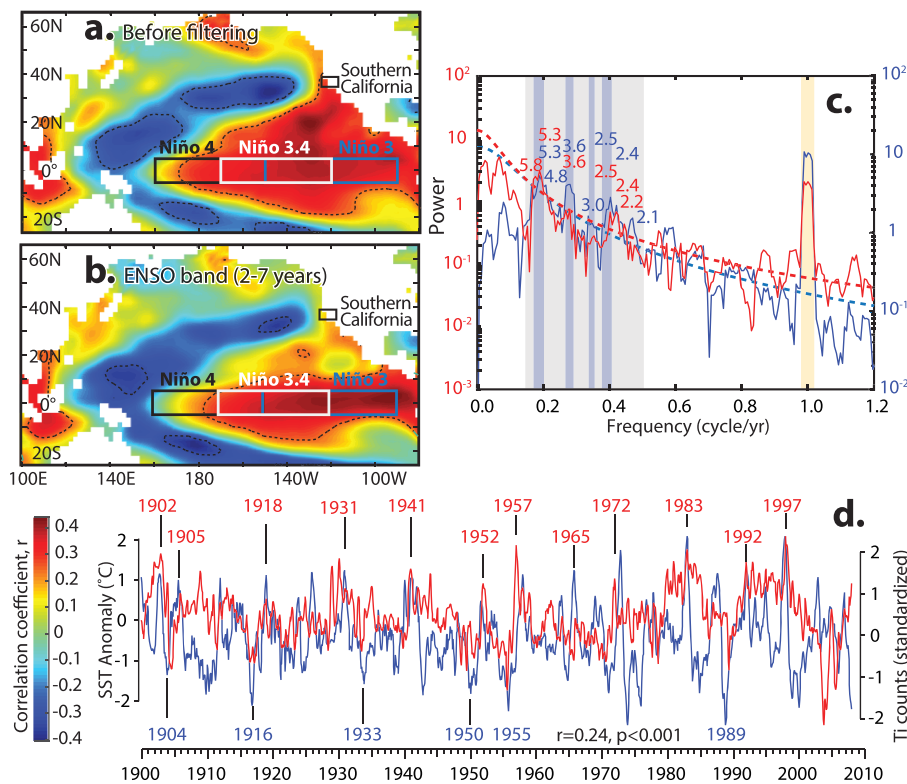


Figure 1. Field correlation of extended winter (November–April) SST in the tropical and northern Pacific with (a) average, and (b) ENSO band (2–7 years) filtered extended winter (November–April) precipitation in Southern California from 1900–2013. The black dashed contour encloses regions significantly correlated ($p < 0.013$) with Southern California precipitation. Monthly SST data (2° spatial resolution, 26°S to 66°N, 100°E to 100°W) are from the version 4 of NOAA extended reconstructed sea surface temperature (Huang et al., 2015) (NOAA_ERSST_V4 data from <http://www.esrl.noaa.gov/psd/>). Average monthly southern California precipitation data (0.5° spatial resolution, 32°N to 36°N, 122°W to 114°W, white dashed box) are taken from the GPCC Full Data Reanalysis version 6 (Schneider et al., 2014). Santa Barbara Basin (SBB; red star), Niño 1 + 2 (white box: 0–10°S, 80°–90°W), Niño 3 (blue box: 5°N to 5°S, 150°–90°W), Niño 3.4 (black box: 5°N to 5°S, 170°–120°W), and Niño 4 (white box: 5°N to 5°S, 160°E to 150°W) (Trenberth & Stepaniak, 2001) are displayed. (c) Comparison of Ti time series from SPR0901-04BC (red line) and Niño 3.4 SST (blue line) from 1900 to 2008. (d) 2π prolate multitaper power spectrum of the annually tuned SPR0901-04BC Ti time series compared to the Niño 3.4 SST monthly time series from 1900 to 2008 (Rayner et al., 2003) (data source: http://www.esrl.noaa.gov/psd/gcos_wgsp/Timeseries/Nino34/). Periods exceeding the 95% confidence level of classical red noise modeling are labeled. Orange shading represents a $\pi/4$ phase lead/lag and the dashed line indicates no phase difference. All the significant signals ($\geq 95\%$ confidence level) produced by multitaper power spectrum (Figure S4a), with coherency above 95% confidence level (Figure S4b) and phase lag (Figure S4c) within $\pi/4$ (equals 1.5 years for annual cycle) are marked with purple bars. The annual signal is indicated by a yellow bar. Niño 3.4 SST data (5°S to 5°N and 170°–120°W average area) were calculated from the HadISST1 (Hadley Centre Sea Ice and Sea Surface Temperature data set).

correlation coefficient ($r = 0.30, p < 0.01$) was found between the Niño 3.4 and the annually tuned 04BC Ti time series from 1900 to 2008 after a 2- to 7-year bandpass filter was applied (Figure S2). Multitaper method (MTM) spectrum analysis (Figure 1d) was then employed with the same data sets. The 04BC Ti time series contains significant (95%) spectral peaks in the ENSO band (2–7 years) corresponding to 5.8-, 5.3-, 3.6-, 2.5-, 2.4-, and 2.2-year periods consistent with Niño 3.4 SST, which contains significant (95%) peaks at 5.3, 4.8, 3.6, 3.0, 2.5, 2.4, and 2.1 years (Figure 1c). Cross-spectral analysis between the records reveals that all signals with coherency above the 95% significance level and phase lag within $\pi/4$ (equals 1.5 years for an annual cycle) fall within ENSO band (at 5.3, 3.6, 3.0, and 2.5 years, indicated by vertical purple bars) (Figures S3b and S3c). Thus, the relationship between interannual precipitation variability in Southern California and tropical ENSO forcing remains after river runoff sediments are deposited in SBB.

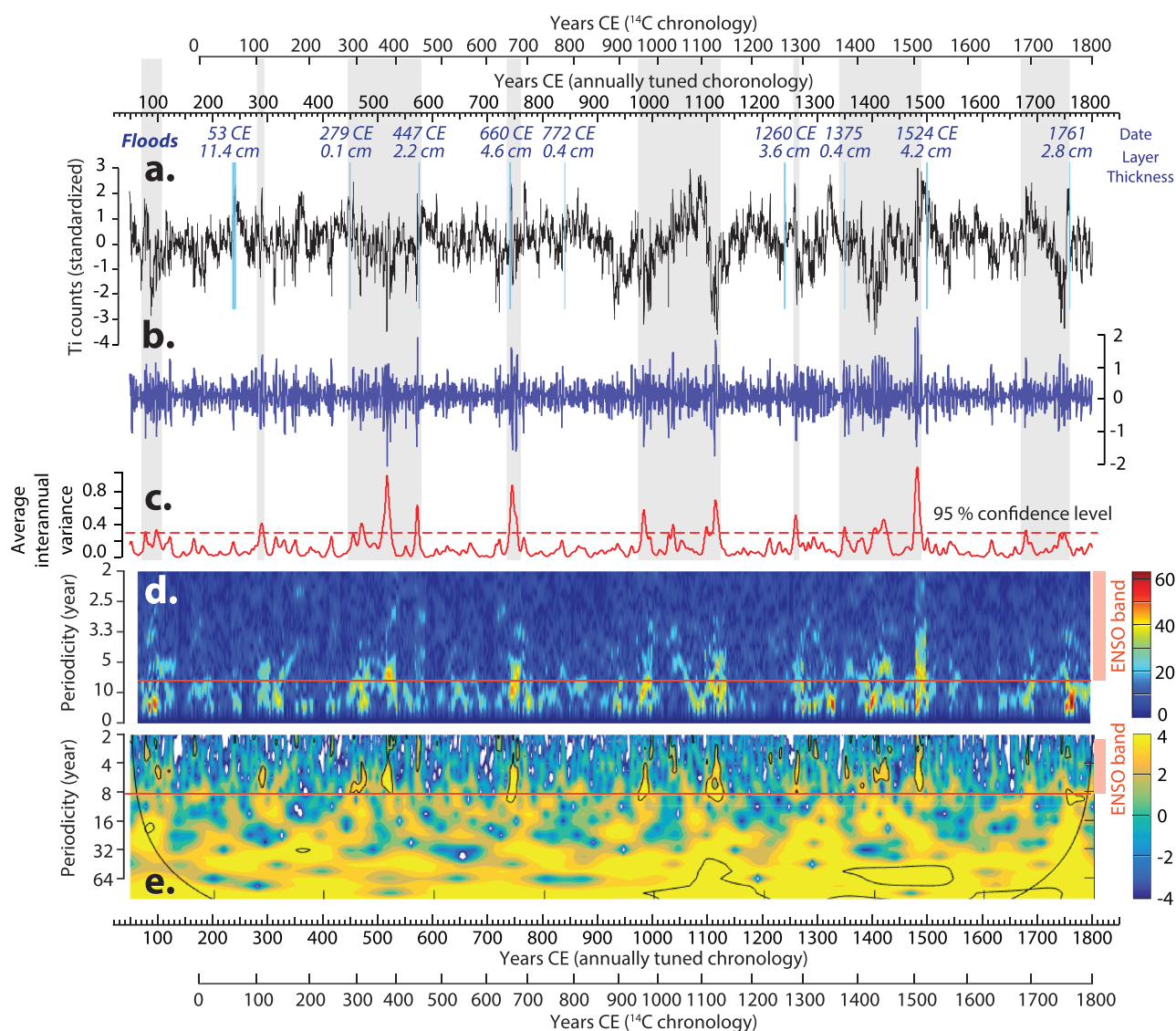


Figure 2. (a) The annually tuned SPR0901-03KC Ti time series (black line) after prewhitening by subtracting the LOESS (locally estimated scatterplot smoothing) curve (with window equal to the length of the Ti time series) curve. Blue bars indicate flood layers. (b) Interannual precipitation variance of (a) isolated by applying a 2- to 7-year Taner bandpass filter. (c) Scale-average wavelet power spectrum over 2–7 years for the Ti time series (red line). Dashed red line is the 95% confidence level. (d) Evolutionary FFT power spectrogram of the Ti time series with a 20-year sliding window. Power is not normalized per spectrum, with the highest power in dark red and the lowest in dark blue. (e) Wavelet analysis of the Ti time series. The thick contour encloses regions of >95% confidence for a red-noise process with a lag-1 coefficient. Gray shading represents intervals with strong interannual variability of the Ti time series.

3. Interannual Precipitation Variability in Southern California During the Common Era

Southern Californian hydroclimate has varied significantly over the past 2,000 years (Cook et al., 2010; Kirby et al., 2014). High Ti counts in SBB (Figure 2a), lake high stands (Hiner et al., 2016; Kirby et al., 2010; Kirby et al., 2012; Kirby et al., 2014), and the regional Palmer drought severity index tree ring records (Cook et al., 2010) indicate that the Californian hydroclimate was wetter during the Little Ice Age (after 1300). Two megadroughts (~830–1075 and 1120–1300) during the Medieval Climate Anomaly associated with lake low stands (Stine, 1994) and identified in tree rings (Cook et al., 2010) and low Ti in SBB suggest a drier hydroclimate. Previous studies have asserted that a wetter Southern California hydroclimate implies a sustained El Niño-like ocean-atmosphere pattern while the megadroughts were associated with a cool La Niña-like state in the equatorial Pacific (Cook et al., 2010; Seager et al., 2008). But recent research has

emphasized that changes in interannual ENSO variance, instead of long-duration La Niña-like mean states, contributed to megadrought occurrence (Coats et al., 2015; Coats, Smerdon, Cook, et al., 2016; Coats, Smerdon, Karnauskas, & Seager, 2016; Parsons & Coats, 2019; Steiger et al., 2019; Stevenson et al., 2015).

The high-resolution SBB Ti record reveals changes of interannual precipitation variability in Southern California over the Common Era, including during megadroughts and the Little Ice Age. Employing MTM power spectrum analysis to explore 2,000 years of interannual variability in the Ti time series, significant peaks (>95% confidence level) are observed at 8.1-, 6.3-, 5.4-, 4.6-, 3.6-, 3.3-, 3.0-, 2.3-, and 2.1-year periods (Figure S4). However, the power of these periodicity peaks changes within the 2- to 7-year ENSO band throughout the last 2,000 years (Figure S5). Wavelet spectrum analysis and an evolutionary fast Fourier transform power spectrogram (Kodama & Hinnov, 2015) of the Ti time series shows significant (black contours in Figure 2e) power in the 2- to 7-year ENSO band between 280–400, 650–680, 940–980, 1000–1140, 1270–1290, 1500–1520, and 1750–1770 (based on ^{14}C chronology). Increased interannual variance based on the scale-averaged wavelet analysis of the Ti time series occurs between ~100–120, 280–460, 650–680, 950–1140, 1270–1290, 1370–1520, and 1680–1770, while decreased variance occurs between ~150–280, 500–600, 700–950, 1150–1270, and 1550–1680 (based on ^{14}C chronology) (Figure 2c). The weak Ti interannual variance between 700–950 and 1150–1270 (Figure 2) generally overlaps with megadroughts (~830–1075 and 1120–1300) indicated by reconstructed PDSI (Cook et al., 2010). Exceptions occurred at 950–980, 1020–1040, and 1110–1140 as multidecadal droughts terminated and may be associated with extreme precipitation events that shifted the hydroclimate state from dry to wet. For example, in the 20th-century, the 6-year drought in Santa Barbara County from 1986 to 1991 ended with precipitation events associated with the 1991–1992 El Niño event. Interannual precipitation variance was not consistent during the Little Ice Age: High variance was observed between 1370–1520 and 1680–1770, while low variance dominated 1540–1680 (Figure 2).

4. Interannual Precipitation Variability in Southern California and ENSO

In the eastern equatorial Pacific, long hydroclimate records from the well-dated, low-resolution El Junco Lake in the Galápagos Islands (Conroy et al., 2008) show intensified precipitation between ~200–450 and 600–750 (Figure 3a), reflecting higher ENSO variance along with more ENSO events. Given age model and resolution uncertainties, this result agrees with the greater interannual precipitation variance recorded in SBB between 280–460 and 650–680 (Figure 3e). However, the relationship between SBB and eastern equatorial Pacific records breaks down during the last millennium: Higher interannual precipitation variance was observed in SBB between 1370–1520 and 1680–1770, while ENSO variance recorded in Galápagos Islands was weak during these two intervals (Figure 3). Such inconsistencies between records could be related to the distinct teleconnection patterns of Eastern Pacific and Central Pacific El Niño events. Eastern Pacific El Niños, characterized by SST anomalies in the eastern equatorial Pacific, more likely contribute to heavy precipitation in the eastern equatorial Pacific by intensifying convection locally, while central Pacific El Niños, characterized by warming in the Niño 3.4 and 4 regions, are more closely associated with a stronger, south-shifted jet stream (Mo, 2010; Parsons & Coats, 2019; Weng et al., 2009; Yu & Zou, 2013) that brings tropical moisture to Southern California.

Increased interannual variance in Southern California precipitation between 1370–1520 and 1680–1770 suggests greater ENSO variance or a stronger ENSO teleconnection between the tropical Pacific and North America. In the western Pacific, tree-ring cellulose $\delta^{18}\text{O}$ from Taiwan (Figure S6d) suggests higher central Pacific ENSO variance between ~1350 and 1600 (Liu et al., 2017). The tree ring-based North American Drought Atlas (Figure S6d) also indicates increased ENSO variance between ~1400 and 1800 (Li et al., 2011). Well-dated decadal to centennial coral records with monthly resolution from Christmas and Palmyra Islands (Figure 3b) in the central tropical Pacific indicate higher ENSO variance during 1516–1561 and 1635–1703 (Cobb et al., 2003; Cobb et al., 2013). $\delta^{18}\text{O}$ of individual *G. ruber* shells from Galápagos marine sediments (Figure S6e) suggests increased ENSO activity after ~1500 (Rustic et al., 2015). Additionally, increased variability of reconstructed Niño 3.4 SST between ~1450 and 1550 was reported (Figure S6f) (Emile-Geay et al., 2013). Taken together, the above high-resolution ENSO records from the tropical Pacific suggest increased ENSO variance since ~1350, while interannual precipitation variance recorded from SBB is weak during 1540–1680 (Fig S5). Thus, SBB interannual precipitation variance is

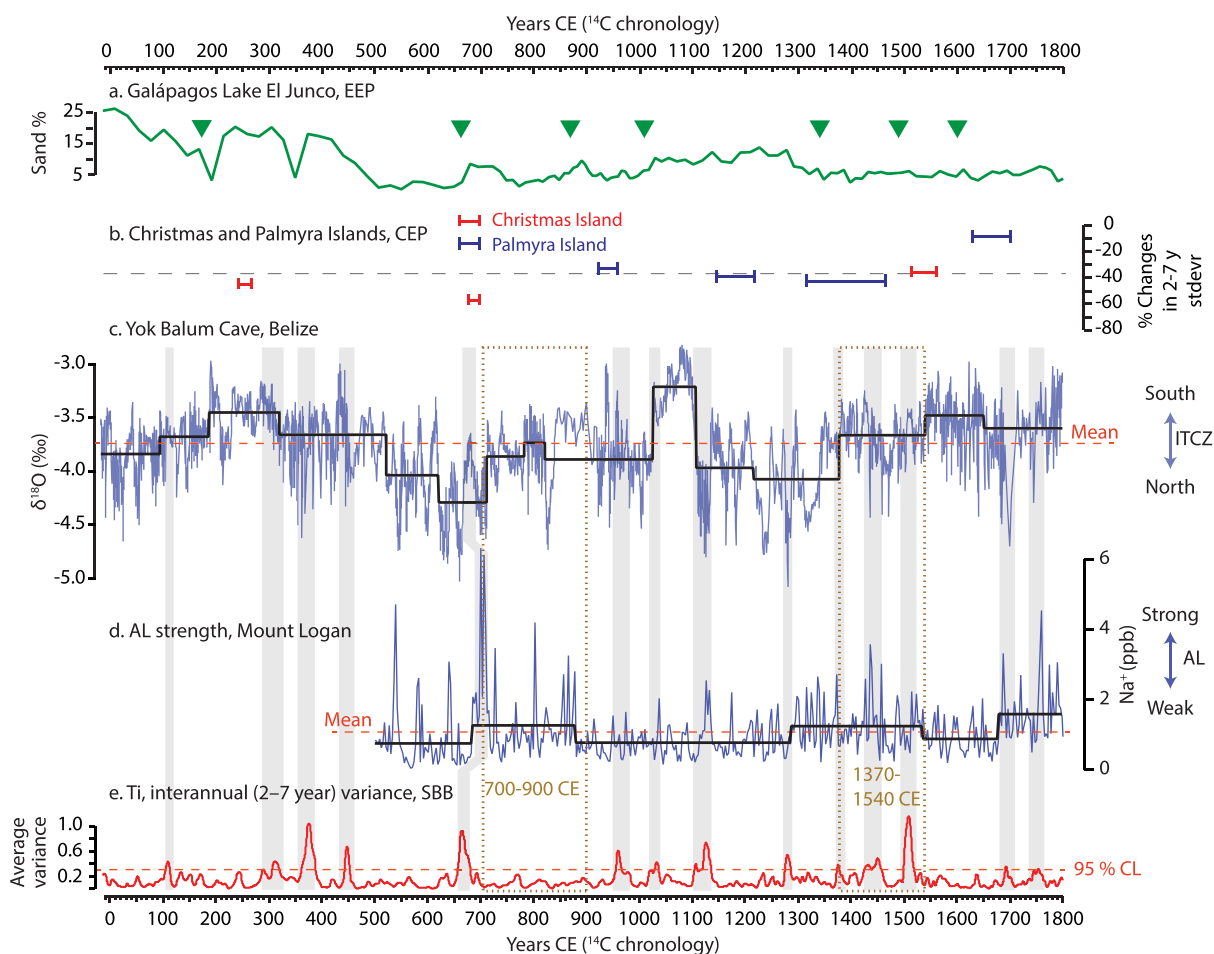


Figure 3. Southern California interannual precipitation compared to ITCZ migration, AL strength and ENSO variance strength in other ENSO reconstructions. (a) Sand abundance from lake El Junco (Conroy et al., 2008) Galápagos. (b) Relative ENSO variance (SD of the 2- to 7-year band, plotted as percent difference from 1968–1998) of fossil coral $\delta^{18}\text{O}$ from Palmyra (blue) and Christmas (red) Islands, central Pacific Ocean (Cobb et al., 2003; Cobb et al., 2013). (c) Yok Balum Cave $\delta^{18}\text{O}$ speleothem, Belize (Kennett et al., 2012), indicating the ITCZ position. (d) Mount Logan annual Na^+ concentration (ppb) indicating wintertime AL strength (Osterberg et al., 2014). Mean values are shown with dashed red line. Regime shifts were detected using SRSD (black lines). (e) Scale-averaged interannual precipitation variance over 2–7 years of the standardized SPR0901-03KC Ti counts from this study. The 95% confidence level is shown with red dashed lines. Intervals with strong ENSO variance are indicated by gray bars.

not only driven by ENSO variance in the tropical Pacific; we hypothesize that the strength and position of midlatitude pressure systems in the North Pacific could be modulating the ENSO teleconnection between the tropical Pacific and North America.

5. The ENSO Teleconnection in the Northeastern Pacific

As the west coast of North America is not located in an ENSO SSTAA core region, tropical climate influences precipitation in Southern California through an ENSO teleconnection. Although the teleconnection strength increases with the amplitude of tropical Pacific SST anomalies (Diaz et al., 2001), the position and strength of extratropical pressure systems may complicate ENSO variance recorded in SBB. An intensified AL, associated with the southeastward shift of the low-pressure center (AL) and North Pacific Jet Stream (Rodionov et al., 2007), allows warm, moist air advection onto the West Coast, enhancing the tropical and midlatitude Pacific climate coupling (Osterberg et al., 2014). The resulting intensified ENSO teleconnection increases Southern California's sensitivity to ENSO. When the AL is weak, the North Pacific High intensifies and shifts northward, creating a persistent high-pressure ridge and preventing moisture from reaching

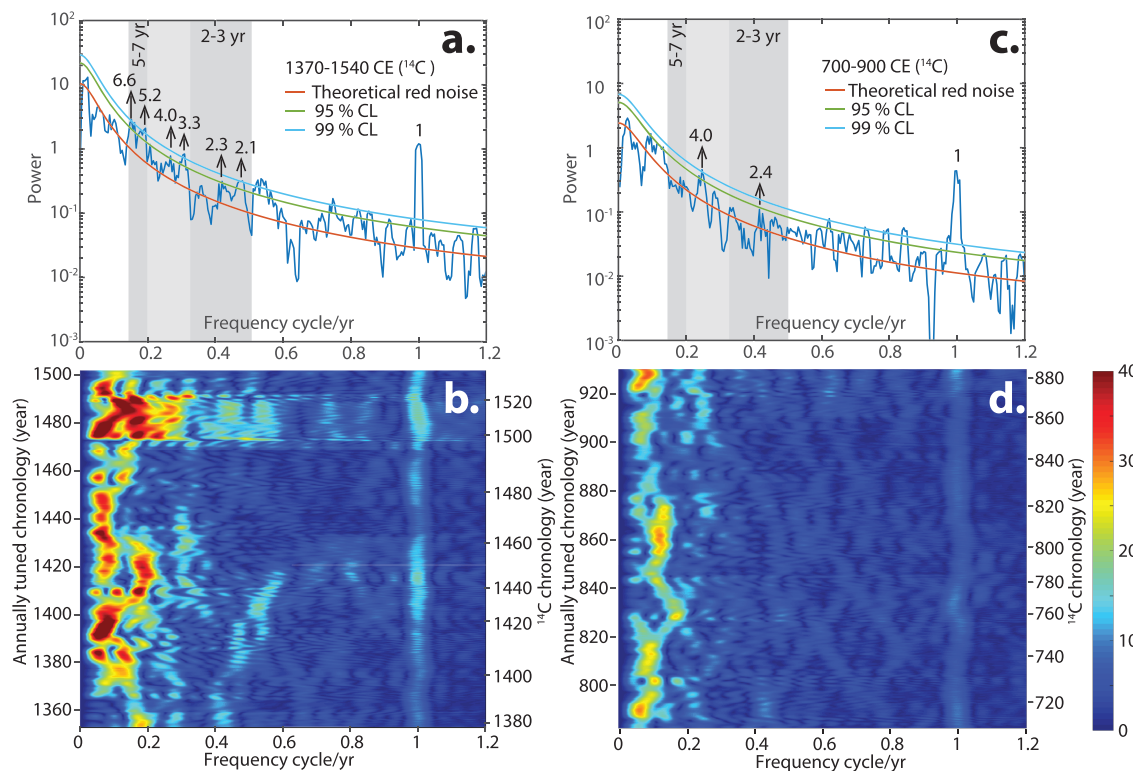


Figure 4. 2π prolate multitaper power spectrum of two selected intervals from the SPR0901-03KC Ti time series from SBB: (a) 1370–1540 CE and (c) 700–900 CE. The two intervals are dated using the ^{14}C chronology, while the duration of both intervals is 167 years according to the annually tuned chronology. Shaded areas represent the ENSO band (2–7 years). Confidence levels are shown with significant spectral peaks ($\geq 95\%$ confidence level) labeled in years. Evolutionary FFT power spectrogram of Ti time series over (b) 1370–1540 CE and (d) 700–900 CE with a 20-year sliding window. Power is not normalized per spectrum for either series. The highest power is in dark red, and the lowest is in dark blue.

Southern California (Rodionov et al., 2007; Wang et al., 2014). The resulting weak ENSO teleconnection consequently would suppress interannual precipitation variance recorded in SBB.

A comparison of AL strength and Southern Californian interannual precipitation variability records through Sequential Regime Shift Detection (Rodionov, 2004) supports the influence of shifting pressure system patterns on the strength of the ENSO teleconnection to SBB. A sea salt (Na^+) record from the Mount Logan ice core from Alaska (Osterberg et al., 2014) records changes in AL strength in the eastern Pacific during the past 1,200 years (Figure 3d). A weak AL between 1540 and 1680 (Figure 3d) is coincident with increased ENSO variance recorded by tropical Pacific proxies (Cobb et al., 2003; Cobb et al., 2013; Liu et al., 2017; Moy et al., 2002; Rustic et al., 2015), when reduced interannual precipitation variance was observed in SBB (Figure 3). This suggests that a weak ENSO teleconnection may suppress the sensitivity of the Southern California hydroclimate to ENSO activity in the tropical Pacific, leading to damped interannual precipitation variance.

The migration of the ITCZ also potentially impacts ENSO variance in the tropical Pacific; a northward shift of the ITCZ strengthens the interhemispheric and equatorial Pacific zonal SST gradient, contributing to stronger cross-equatorial trade winds and reduced ENSO variance, while a southward shift of the ITCZ results in greater ENSO variance (Chiang et al., 2008; Rustic et al., 2015). A high-resolution, well-dated speleothem $\delta^{18}\text{O}$ record from Yok Balum Cave, Belize (Kennett et al., 2012), provides a subannually resolved precipitation archive mainly driven by ITCZ displacement over the last two millennia (Figure 3c). We compared this ITCZ-related precipitation reconstruction with intervals when the ENSO teleconnection in California was strong. Both 700–900 and 1370–1540 (^{14}C chronology; the duration of both intervals is 167 years within the annually tuned chronology) are characterized by a strong AL, minimizing the changing ENSO teleconnection influence on interannual precipitation in southern California. MTM spectrum analysis shows that during 1370–1540, when ITCZ shifted southward, interannual precipitation variance was

higher with longer periodicity (5–7 years, Figures 4a and 4c), while when ITCZ moved northward in 700–900, the interannual precipitation variance was reduced with shorter periodicity (2–4 years, Figures 4b and 4d). This result suggests that a southward shift of the ITCZ contributes to stronger and longer-period ENSO events in our record of Southern California's hydroclimate.

The correlation between ITCZ migration and the amplitude/frequency of ENSO has also been observed in modern observations and model simulations. A 20% ENSO amplitude reduction over the last decade has been linked to a northward-displaced ITCZ and stronger cross-equatorial winds (Hu & Fedorov, 2018). Relative to 1950–1970, the ITCZ shifted southward in 1980–2000, causing the boreal spring to begin earlier and end later and allowing more time for ENSO development, which could result in stronger El Niño events with longer periods (Fang et al., 2008).

Therefore, both ITCZ position and AL strength may influence the interannual precipitation variability in Southern California. From 0–500 CE, the ITCZ shifted southward, potentially leading to higher ENSO variance in the tropical Pacific, as indicated by the ENSO record from Galápagos Lake sediments (Figure 3a). High interannual precipitation variance was found in SBB between 280 and 460 (Figure 3e), which may support a strong ENSO teleconnection associated with enhanced AL. The Mount Logan AL record, however, does not extend to 0–500 CE, preventing the evaluation of the impact of AL strength on interannual precipitation in Southern California. The northern position of the ITCZ between 500 and 660 possibly caused the weak ENSO variance recorded in the Galápagos islands (Figures 3a and 3c). Such reduced ENSO variance in the tropical Pacific, together with a weak ENSO teleconnection to Southern California, resulting from a weak AL between 500 and 660 (Figure 3c), appears to have led to persistent low interannual precipitation variance in Southern California (Figure 3e). The isolated interannual variance peak at 660–680 coincides with an extremely strong AL interval around 690–720. The ITCZ remained in a northerly position from 900–1370, except for a southward shift between 1020 and 1110 (Figure 3c). This migration of ITCZ is also supported by a Kiritimati lake record in the central tropical Pacific, which indicates a northward ITCZ position from ~900–1200 and a southward shift between ~1000 and 1050 (Higley et al., 2018). The weak interannual Ti variability during ~700–900, concurrent with a strong AL (Figure 3d), could be related to reduced ENSO variance in the tropical Pacific as suggested by the El Junco Lake sediment in Galápagos (Figure 3a). The AL was weak between 880 and 1280 (Figure 3d). The generally low interannual Southern California precipitation variance between 1150 and 1280 is best explained by a weakened ENSO variance in the tropical Pacific and/or suppressed ENSO teleconnection between the tropical Pacific and Southern California. Intervals of increased interannual precipitation variance during 950–1140 are related to the transition between dry and wet hydroclimate concurrent with the significant shift of ITCZ. The transient high ENSO variance at ~1280 might be associated with the 1257 Samalas volcanic eruption (Gao et al., 2012) that impacted the winter of 1258, ahead of an extreme El Niño event (Emile-Geay et al., 2008). Thus, interannual precipitation in Southern California is driven by tropical ENSO variance but is also modulated by extratropical pressure systems at multidecadal to centennial scales through ENSO teleconnections.

6. Conclusions

Interannual precipitation variability in Southern California is closely related to SST in the tropical Pacific via an ENSO teleconnection. Subannually resolved ITRAX scanning XRF Ti counts from SBB were used to reconstruct Southern California hydroclimate during the past two millennia and indicate that interannual precipitation variability responds closely to the interactions between tropical and extratropical climate forcing. After ~1350, when paleoclimate records suggest that the ITCZ shifted southward, interannual precipitation variance in Southern California increased, except for a ~100-year interval (1550–1680), when a weak AL was recorded at Mount Logan. Given other ENSO records from the tropical Pacific indicate increased ENSO variance after 1350, the depressed interannual precipitation variability in Southern California from 1550 to 1680 might be associated with a weak ENSO teleconnection caused by a weaker AL. Extra-tropical pressure system activity could therefore influence the interannual precipitation variability in Southern California by modulating the ENSO teleconnection between the tropical Pacific and North America. Two 200-year intervals associated with a robust ENSO teleconnection created by strong AL were selected to minimize the impact of midlatitude pressure systems on precipitation and therefore explore the possible forcing of tropical Pacific ENSO variance on Southern California hydroclimate. Interannual precipitation variance

in Southern California increased when the ITCZ migrated southward (1370–1540 CE), accompanied by longer periodicities (5–7 years). Weak interannual precipitation variance with shorter periodicity (2–3 years) was observed when ITCZ shifted northward (700–900 CE). Therefore, interannual precipitation in Southern California is driven by tropical ENSO variance via the ENSO teleconnection but is also modulated by extratropical pressure systems and influenced by the position of ITCZ. This research contributes to our understanding of the hydroclimate changes in Southern California and the stationarity of the ENSO teleconnection to this region.

Funding

This work was funded by the National Science Foundation OCE-0752093 and OCE-1304327 (I. H.) 1542697 and 1303605 (L. H.), 1304148 (E. B.), OCE-0752068 (A. S.), and OCE-0751803 to D. K. P.

Author Contributions

X. D. undertook the statistical analysis and wrote the manuscript, I. H. supervised the work and contributed to the manuscript, L. H. provided statistical expertise, E. B. undertook the scanning XRF analysis, and D. K. P. and A. S. provided core material and sediment expertise.

Competing Interests

The authors declare no competing interests. Data from this work are available at <https://doi.pangaea.de>. Raw XRF data can be found at <https://doi.org/10.7302/6dp2-3767>.

Acknowledgments

We thank the crew of the R/V Robert Gordon Sproul, the Lac-Core staff, and Wally Lingwall for assistance with the scanning XRF data. We would like to thank Julia Cole and Xianglei Huang for helpful comments and discussions. We would also like to thank the two anonymous reviewers for their constructive feedback.

References

- Blaauw, M., & Christen, J. A. (2011). Flexible paleoclimate age-depth models using an autoregressive gamma process. *Bayesian Analysis*, 6(3), 457–474. <https://doi.org/10.1214/11-Ba618>
- Cane, M. A., & Zebiak, S. E. (1985). A Theory for El-Niño and the Southern Oscillation. *Science*, 228(4703), 1085–1087. <https://doi.org/10.1126/science.228.4703.1085>
- Chiang, J. C. H., Fang, Y., & Chang, P. (2008). Interhemispheric thermal gradient and tropical Pacific climate. *Geophysical Research Letters*, 35, L14704. <https://doi.org/10.1029/2008GL034166>
- Coats, S., Smerdon, J. E., Cook, B. I., & Seager, R. (2015). Are simulated megadroughts in the North American Southwest forced? *Journal of Climate*, 28(1), 124–142. <https://doi.org/10.1175/JCLI-D-14-00071.1>
- Coats, S., Smerdon, J. E., Cook, B. I., Seager, R., Cook, E. R., & Anchukaitis, K. J. (2016). Internal ocean-atmosphere variability drives megadroughts in Western North America. *Geophysical Research Letters*, 43, 9886–9894. <https://doi.org/10.1002/2016GL070105>
- Coats, S., Smerdon, J. E., Karnauskas, K. B., & Seager, R. (2016). The improbable but unexceptional occurrence of megadrought clustering in the American West during the Medieval Climate Anomaly. *Environmental Research Letters*, 11(7), 074025. <https://doi.org/10.1088/1748-9326/11/7/074025>
- Cobb, K. M., Charles, C. D., Cheng, H., & Edwards, R. L. (2003). El Niño/Southern Oscillation and tropical Pacific climate during the last millennium. *Nature*, 424(6946), 271–276. <https://doi.org/10.1038/nature01779>
- Cobb, K. M., Westphal, N., Sayani, H. R., Watson, J. T., di Lorenzo, E., Cheng, H., et al. (2013). Highly variable El Niño-Southern Oscillation throughout the Holocene. *Science*, 339(6115), 67–70. <https://doi.org/10.1126/science.1228246>
- Conroy, J. L., Overpeck, J. T., Cole, J. E., Shanahan, T. M., & Steinitz-Kannan, M. (2008). Holocene changes in eastern tropical Pacific climate inferred from a Galápagos lake sediment record. *Quaternary Science Reviews*, 27(11–12), 1166–1180. <https://doi.org/10.1016/j.quascirev.2008.02.015>
- Cook, E. R., Seager, R., Heim, R. R., Vose, R. S., Herweijer, C., & Woodhouse, C. (2010). Megadroughts in North America: placing IPCC projections of hydroclimatic change in a long-term palaeoclimate context. *Journal of Quaternary Science*, 25(1), 48–61. <https://doi.org/10.1002/jqs.1303>
- Diaz, H. F., Hoerling, M. P., & Eischeid, J. K. (2001). ENSO variability, teleconnections and climate change. *International Journal of Climatology*, 21(15), 1845–1862. <https://doi.org/10.1002/joc.631.abs>
- Du, X., Hendy, I. L., & Schimmelmann, A. (2018). A 9000-year flood history for Southern California: A revised stratigraphy of varved sediments in Santa Barbara Basin. *Marine Geology*, 397, 29–42. <https://doi.org/10.1016/j.margeo.2017.11.014>
- Emile-Geay, J., Cobb, K. M., Mann, M. E., & Wittenberg, A. T. (2013). Estimating central equatorial Pacific SST variability over the past millennium. Part II: Reconstructions and implications. *Journal of Climate*, 26(7), 2329–2352. <https://doi.org/10.1175/JCLI-D-11-00511.1>
- Emile-Geay, J., Seager, R., Cane, M. A., Cook, E. R., & Haug, G. H. (2008). Volcanoes and ENSO over the past millennium. *Journal of Climate*, 21(13), 3134–3148. <https://doi.org/10.1175/2007jcli1884.1>
- Fang, Y., Chiang, J. C. H., & Chang, P. (2008). Variation of mean sea surface temperature and modulation of El Niño-Southern Oscillation variance during the past 150 years. *Geophysical Research Letters*, 35, L14709. <https://doi.org/10.1029/2008GL033761>
- Gao, C. C., Robock, A., & Ammann, C. (2012). Volcanic forcing of climate over the past 1500 years: An improved ice core-based index for climate models. *Journal of Geophysical Research*, 117, D16112. <https://doi.org/10.1029/2012JD018052>
- Haug, G. H., Hughen, K. A., Sigman, D. M., Peterson, L. C., & Rohl, U. (2001). Southward migration of the intertropical convergence zone through the Holocene. *Science*, 293(5533), 1304–1308. <https://doi.org/10.1126/science.1059725>
- Hendy, I. L., Dunn, L., Schimmelmann, A., & Pak, D. K. (2013). Resolving varve and radiocarbon chronology differences during the last 2000 years in the Santa Barbara Basin sedimentary record, California. *Quaternary International*, 310, 155–168. <https://doi.org/10.1016/j.quaint.2012.09.006>

- Hendy, I. L., Napier, T. J., & Schimmelmann, A. (2015). From extreme rainfall to drought: 250 years of annually resolved sediment deposition in Santa Barbara Basin, California. *Quaternary International*, 387, 3–12. <https://doi.org/10.1016/j.quaint.2015.01.026>
- Higley, M. C., Conroy, J. L., & Schmitt, S. (2018). Last millennium meridional shifts in hydroclimate in the Central Tropical Pacific. *Paleoceanography and Paleoclimatology*, 33(4), 354–366. <https://doi.org/10.1002/2017pa003233>
- Hiner, C. A., Kirby, M. E., Bonuso, N., Patterson, W. P., Palermo, J., & Silveira, E. (2016). Late Holocene hydroclimatic variability linked to Pacific forcing: Evidence from Abbott Lake, coastal central California. *Journal of Paleolimnology*, 56(4), 299–313. <https://doi.org/10.1007/s10933-016-9912-4>
- Hu, S., & Fedorov, V. A. (2018). Cross-equatorial winds control El Niño diversity and change. *Nature Climate Change*, 8(9), 798–802. <https://doi.org/10.1038/s41558-018-0248-0>
- Huang, B., Banzon, V. F., Freeman, E., Lawrimore, J., Liu, W., Peterson, T. C., et al. (2015). Extended reconstructed sea surface Temperature Version 4 (ERSST.v4). Part I: Upgrades and Intercomparisons. *Journal of Climate*, 28(3), 911–930. <https://doi.org/10.1175/JCLI-D-14-00006.1>
- Jong, B. T., Ting, M. F., & Seager, R. (2016). El Niño's impact on California precipitation: Seasonality, regionality, and El Niño intensity. *Environmental Research Letters*, 11(5). <https://doi.org/10.1088/1748-9326/11/5/054021>
- Kennett, D. J., Breitenbach, S. F. M., Aquino, V. V., Asmerom, Y., Awe, J., Baldini, J. U. L., et al. (2012). Development and disintegration of Maya political systems in response to climate change. *Science*, 338(6108), 788–791. <https://doi.org/10.1126/science.1226299>
- Kirby, M. E., Feakins, S. J., Hiner, C. A., Fantozzi, J., Zimmerman, S. R. H., Dingemans, T., & Mensing, S. A. (2014). Tropical Pacific forcing of Late-Holocene hydrologic variability in the coastal southwest United States. *Quaternary Science Reviews*, 102, 27–38. <https://doi.org/10.1016/j.quascirev.2014.08.005>
- Kirby, M. E., Lund, S. P., Patterson, W. P., Anderson, M. A., Bird, B. W., Ivanovici, L., et al. (2010). A Holocene record of Pacific Decadal Oscillation (PDO)-related hydrologic variability in Southern California (Lake Elsinore, CA). *Journal of Paleolimnology*, 44(3), 819–839. <https://doi.org/10.1007/s10933-010-9454-0>
- Kirby, M. E., Zimmerman, S. R. H., Patterson, W. P., & Rivera, J. J. (2012). A 9170-year record of decadal-to-multi-centennial scale pluvial episodes from the coastal Southwest United States: A role for atmospheric rivers? *Quaternary Science Reviews*, 46, 57–65. <https://doi.org/10.1016/j.quascirev.2012.05.008>
- Kodama, K. P., & Hinnov, L. A. (2015). Rock magnetic cyclostratigraphy. In *Rock Magnetic Cyclostratigraphy* (pp. 145–156). Chichester: John Wiley & Sons.
- Li, J., Xie, S. P., Cook, E. R., Huang, G., D'Arrigo, R., Liu, F., et al. (2011). Interdecadal modulation of El Niño amplitude during the past millennium. *Nature Climate Change*, 1(2), 114–118. <https://doi.org/10.1038/Nclimate1086>
- Liu, Y., Cobb, K. M., Song, H., Li, Q., Li, C. Y., Nakatsuka, T., et al. (2017). Recent enhancement of central Pacific El Niño variability relative to last eight centuries. *Nature Communications*, 8(1), 15386. <https://doi.org/10.1038/ncomms15386>
- Mann, M. E., Cane, M. A., Zebiak, S. E., & Clement, A. (2005). Volcanic and solar forcing of the tropical Pacific over the past 1000 years. *Journal of Climate*, 18(3), 447–456. <https://doi.org/10.1175/JCLI-3276>
- Mo, K. C. (2010). Interdecadal modulation of the impact of ENSO on precipitation and temperature over the United States. *Journal of Climate*, 23(13), 3639–3656. <https://doi.org/10.1175/2010JCLI3553.1>
- Moy, C. M., Seltzer, G. O., Rodbell, D. T., & Anderson, D. M. (2002). Variability of El Niño/Southern Oscillation activity at millennial timescales during the Holocene epoch. *Nature*, 420(6912), 162–165. <https://doi.org/10.1038/nature01194>
- Napier, T. J., & Hendy, I. L. (2016). The impact of hydroclimate and dam construction on terrigenous detrital sediment composition in a 250-year Santa Barbara Basin record off southern California. *Quaternary International*, 469, 151–168. <https://doi.org/10.1016/j.quaint.2016.07.045>
- Nezlin, N. P., DiGiacomo, P. M., Stein, E. D., & Ackerman, D. (2005). Stormwater runoff plumes observed by SeaWiFS radiometer in the Southern California Bight. *Remote Sensing of Environment*, 98(4), 494–510. <https://doi.org/10.1016/j.rse.2005.08.008>
- Osterberg, E. C., Mayewski, P. A., Fisher, D. A., Kreutz, K. J., Maasch, K. A., Snead, S. B., & Kelsey, E. (2014). Mount Logan ice core record of tropical and solar influences on Aleutian Low variability: 500–1998 AD. *Journal of Geophysical Research: Atmospheres*, 119, 11,189–11,204. <https://doi.org/10.1002/2014JD021847>
- Parsons, L. A., & Coats, S. (2019). Ocean-atmosphere trajectories of extended drought in Southwestern North America. *Journal of Geophysical Research: Atmospheres*, 124, 8953–8971. <https://doi.org/10.1029/2019JD030424>
- Rayner, N. A., Parker, D. E., Horton, E. B., Folland, C. K., Alexander, L. V., Rowell, D. P., et al. (2003). Global analyses of sea surface temperature, sea ice, and night marine air temperature since the late nineteenth century. *Journal of Geophysical Research*, 108(D14), 4407. <https://doi.org/10.1029/2002JD002670>
- Rodionov, S. N. (2004). A sequential algorithm for testing climate regime shifts. *Geophysical Research Letters*, 31, L09204. <https://doi.org/10.1029/2004GL019448>
- Rodionov, S. N., Bond, N. A., & Overland, J. E. (2007). The Aleutian Low, storm tracks, and winter climate variability in the Bering Sea. *Deep-Sea Research Part II-Topical Studies in Oceanography*, 54(23–26), 2560–2577. <https://doi.org/10.1016/j.dsr2.2007.08.002>
- Rustic, G. T., Koutavas, A., Marchitto, T. M., & Linsley, B. K. (2015). Dynamical excitation of the tropical Pacific Ocean and ENSO variability by Little Ice Age cooling. *Science*, 350(6267), 1537–1541. <https://doi.org/10.1126/science.aac9937>
- Schneider, U., Becker, A., Finger, P., Meyer-Christoffer, A., Ziese, M., & Rudolf, B. (2014). GPCC's new land surface precipitation climatology based on quality-controlled in situ data and its role in quantifying the global water cycle. *Theoretical and Applied Climatology*, 115(1–2), 15–40. <https://doi.org/10.1007/s00704-013-0860-x>
- Seager, R., Burgman, R., Kushnir, Y., Clement, A., Cook, E., Naik, N., & Miller, J. (2008). Tropical Pacific forcing of North American medieval megadroughts: Testing the concept with an atmosphere model forced by coral-reconstructed SSTs. *Journal of Climate*, 21(23), 6175–6190. <https://doi.org/10.1175/2008JCLI2170.1>
- Seager, R., Naik, N., Ting, M., Cane, M. A., Harnik, N., & Kushnir, Y. (2010). Adjustment of the atmospheric circulation to tropical Pacific SST anomalies: Variability of transient eddy propagation in the Pacific-North America sector. *Quarterly Journal of the Royal Meteorological Society*, 136(647), 277–296. <https://doi.org/10.1002/qj.588>
- Steiger, N. J., Smerdon, J. E., Cook, B. I., Seager, R., Williams, A. P., & Cook, E. R. (2019). Oceanic and radiative forcing of medieval megadroughts in the American Southwest. *Science Advances*, 5(7). <https://doi.org/10.1126/sciadv.aax0087>
- Stevenson, S., Timmermann, A., Chikamoto, Y., Langford, S., & DiNezio, P. (2015). Stochastically generated North American megadroughts. *Journal of Climate*, 28(5), 1865–1880.
- Stine, S. (1994). Extreme and persistent drought in California and Patagonia during medieval time. *Nature*, 369(6481), 546–549. <https://doi.org/10.1038/369546a0>

- Trenberth, K. E., Branstator, G. W., Karoly, D., Kumar, A., Lau, N. C., & Ropelewski, C. (1998). Progress during TOGA in understanding and modeling global teleconnections associated with tropical sea surface temperatures. *Journal of Geophysical Research*, 103(C7), 14,291–14,324. <https://doi.org/10.1029/97JC01444>
- Trenberth, K. E., & Stepaniak, D. P. (2001). Indices of El Niño evolution. *Journal of Climate*, 14(8), 1697–1701. [https://doi.org/10.1175/1520-0442\(2001\)014<1697:Lioeno>2.0.Co;2](https://doi.org/10.1175/1520-0442(2001)014<1697:Lioeno>2.0.Co;2)
- Wang, S. Y., Hipps, L., Gillies, R. R., & Yoon, J. H. (2014). Probable causes of the abnormal ridge accompanying the 2013–2014 California drought: ENSO precursor and anthropogenic warming footprint. *Geophysical Research Letters*, 41, 3220–3226. <https://doi.org/10.1002/2014GL059748>
- Weng, H. Y., Behera, S. K., & Yamagata, T. (2009). Anomalous winter climate conditions in the Pacific rim during recent El Niño Modoki and El Niño events. *Climate Dynamics*, 32(5), 663–674. <https://doi.org/10.1007/s00382-008-0394-6>
- Yu, J. Y., & Zou, Y. H. (2013). The enhanced drying effect of Central-Pacific El Niño on US winter. *Environmental Research Letters*, 8(1). <https://doi.org/Artn01401910.1088/1748-9326/8/1/014019>